Nuclear Quadrupole Resonances of $AlBr_3 \cdot SbBr_3$, $AlI_3 \cdot SbI_3$, and $AlBr_3 \cdot BiBr_3$

Tsutomu OKUDA, Koji YAMADA, Hideta ISHIHARA, and Hisao NEGITA

Department of Chemistry, Faculty of Science, Hiroshima University, Hiroshima 730

(Received May 30, 1977)

The quadrupole coupling constants (e^2Qq/h) and the principal axes of electric field gradient (efg) at ^{81}Br, ^{127}I, ^{27}Al, ^{121}Sb, and ^{209}Bi in $AlBr_3 \cdot SbBr_3$, $AlI_3 \cdot SbI_3$, and $AlBr_3 \cdot BiBr_3$ were determined by means of NQR or NMR, in order to clarify the structures and chemical bonds of these compounds. The NQR spectra of $AlBr_3 \cdot SbBr_3$ and $AlI_3 \cdot SbI_3$ resemble each other and these two compounds consist of V-shaped SbX_2^+ and distorted tetrahedral AlX_4^- ions (X=Br and I). However, there are weak bonds between the Sb atom in SbX_2^+ and the halogens in AlX_4^- ion. The V-shaped SbX_2^+ has the bond angle 97.3° for the bromide and 99.0° for the iodide. The orientation of the efg axes at the ^{121}Sb atom suggests that the antimony atom has a lone pair of electrons in the opposite direction to the bisector of the two Sb–X bonds. On the other hand, only one terminal bromine atom bonded to the Bi atom was found for $AlBr_3 \cdot BiBr_3$.

The formation of the 1:1 adducts between trihalides of the metals of group III and V such as $AlX_3 \cdot SbX_3$ or $GaX_3 \cdot SbX_3$ (X=Cl, Br, or I) has been reported in the literature.[1–3] According to the electron diffraction study, $AlBr_3 \cdot SbBr_3$ has an ethane-like structure (Br_3Sb–$AlBr_3$) in the gaseous state.[4] In the solid state, however, no crystal structure for these compounds has been reported so far. Recently, Chemouni and Potier studied vibrational spectra of the $GaX_3 \cdot SbX_3$ (X=Cl, Br, or I) compounds in the solid state and concluded that the bridging structure (X_2Sb–X–GaX_3) is more probable than the ethane-like structure (X_3Sb–GaX_3).[5]

In the present investigation we discuss the structure and chemical bonds for the adducts $AlBr_3 \cdot SbBr_3$, $AlI_3 \cdot SbI_3$, and $AlBr_3 \cdot BiBr_3$, on the basis of the quadrupole coupling constants and the orientation of the principal axes of the electric field gradient (efg). A part of this work has already been reported elsewhere.[6]

Experimental

Adducts $AlBr_3 \cdot SbBr_3$, $AlI_3 \cdot SbI_3$, and $AlBr_3 \cdot BiBr_3$ were prepared from the stoichiometric mixture of the relevant halides in a sealed tube and crystallized slowly from the melt. The single crystals of these compounds were grown by the Bridgman-Stockbarger method. The NQR spectrometer was a super-regenerative type, and signals were observed on an oscilloscope. The Zeeman effect on the NQR was examined by means of the zero-splitting cone method.[7] The quadrupole coupling constants of ^{27}Al were determined by use of a broad line NMR spectrometer operated at 13.000 MHz. Using single crystals of these compounds, the shift of the central line ($-1/2 \leftrightarrow +1/2$) due to the second order quadrupole effect were observed and analyzed by the Volkoff method.[8,9]

TABLE 1. NQR PARAMETERS OF $AlBr_3 \cdot SbBr_3$, $AlI_3 \cdot SbI_3$, AND $AlBr_3 \cdot BiBr_3$ (296 K)

Compound		ν_1/MHz	ν_2/MHz	ν_3/MHz	ν_4/MHz	$\eta^{a)}$	$\eta^{b)}$	e^2Qq/h/MHz
	^{121}Sb	97.406	113.30			0.817	0.821	415.9
	$^{81}Br(1)$	76.637				0.543		146.6
	Br(2)	79.088				0.477		152.5
$AlBr_3 \cdot SbBr_3$	Br(3)	81.930				0.307		161.3
	Br(4)	82.689				0.141		164.8
	Br(5)	143.63				0.024		287.2
	Br(6)	149.99				0.011		300.0
	^{121}Sb	75.681	94.832			0.742	0.736	343.2
	$^{127}I(1)$	118.18	200.48			0.371	0.382	686.6
	I(2)	118.86	232.68			0.129	0.130	778.2
$AlI_3 \cdot SbI_3$	I(3)	123.04	201.73			0.428	0.426	694.9
	I(4)	123.19	214.40			0.347	0.347	731.1
	I(5)	186.88	373.79			0.014	0.00	1246
	I(6)	207.39	414.40			0.029	0.027	1382
	^{209}Bi	36.941	46.126	72.422	97.364		0.271	587.2
	$^{81}Br(1)$	75.691				0.204		150.3
	Br(2)	76.760				0.868		137.2
$AlBr_3 \cdot BiBr_3$	Br(3)	81.003				0.526		155.0
	Br(4)	83.937				0.426		163.0
	Br(5)	95.316				0.539		182.0
	Br(6)	148.30				0.027		296.6

a) These values were determined by Zeeman effect experiments.

b) These values were determined by the use of frequency ratios, ν_1/ν_2.

Results and Discussion

Tables 1 and 2 show the quadrupole coupling constants (e^2Qq/h) and the asymmetry parameter (η) of the efg tensors observed for ^{81}Br, ^{121}Sb, ^{127}I, ^{209}Bi, and ^{27}Al. These parameters were determined by NQR or NMR experiments using single crystals. The NQR lines of ^{79}Br and ^{123}Sb were also observed at the frequencies expected from the quadrupole moment ratios, $Q(^{79}Br)/Q(^{81}Br)=1.1971$ and $Q(^{123}Sb)/Q(^{121}Sb)=1.2748$.

Table 2. Quadrupole coupling constants for ^{27}Al

Compound	e^2Qq/h/MHz	η	Temp/K
$AlBr_3 \cdot SbBr_3$	7.2±0.1	0.56±0.03	295
$AlI_3 \cdot SbI_3$	5.7±0.1	0.55±0.03	285
$AlBr_3 \cdot BiBr_3$	4.0±0.1	0.32±0.03	295
Al_2Br_6[a]	13.5635	0.7476	298.2
KAl_2Br_7[b]	10.4±0.1	0.19±0.03	284
	8.7±0.1	0.09±0.02	

a) Ref. 19. b) Ref. 9.

$AlBr_3 \cdot SbBr_3$. It is apparent from Table 1 that the bromine atoms are divided into two groups. The first group contains Br(1), Br(2), Br(3), and Br(4), and the second group Br(5) and Br(6). Bromine atoms in the first group have large η values and their e^2Qq/h values are approximately the same as those of $AlBr_4^-$ in $MAlBr_4$ (M=Li, Na, or Cs).[9] These four Br atoms can be assigned to $AlBr_4^-$ ions in the present compound, although most of them have strong interactions with neighboring atoms. Bromine atoms in the second group have very small η values and slightly higher quadrupole coupling constants than those due to the bromines in $SbBr_3$.[10] On the basis of these parameters, Br(5) and Br(6) are considered to form bonds with an antimony atom and they have no interactions with other neighboring atoms, thus differing from the Br atoms in the $SbBr_3$ crystal. Figure 1 shows the zero-splitting patterns which are considered to arise from the Sb and Br atoms in one $SbBr_2$ unit. In practice, however, a pair of zero-splitting patterns was observed for each resonance line; these patterns were symmetrical with respect to the b-axis because of the monoclinic system. It is reasonable to assume that the efg z-axis of the Br(5) or Br(6) atom lies along its Br–Sb bond because of the small η. The bond angle $\angle$BrSbBr determined in this way is 97.3°, which is nearly equal to that of the $SbBr_3$ crystal. In the case of ^{121}Sb ($I=5/2$), the locus of the zero-splitting for ν_1 is formed around

Table 3. NQR parameters of $SbBr_3$, SbI_3, and $BiBr_3$

Compound		η/%	e^2Qq/h/MHz	Temp/K	Ref.
$SbBr_3$	^{81}Br	6.8—8.0	273.6[a]	292.5	10
	^{121}Sb	8.3	319.9	304	20
SbI_3	^{127}I	56.5	895.8	77	20
	^{121}Sb	0	169.4	77	20
$BiBr_3$	^{81}Br	7.7—42.4	223.5[a]	298	18
	^{209}Bi	82.8	266.6	289	18

a) Averaged values of three resonance lines.

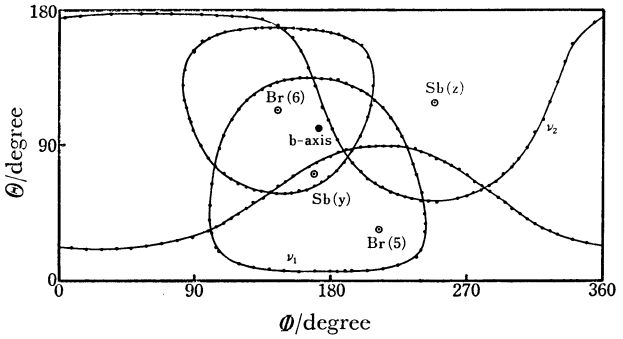

Fig. 1. Zero-splitting loci for the $^{81}Br(5)$, $^{81}Br(6)$, $^{121}Sb(\pm1/2 \leftrightarrow \pm3/2)$, and $^{121}Sb(\pm3/2 \leftrightarrow \pm5/2)$ lines in the $AlBr_3 \cdot SbBr_3$ crystal at room tempreature. In practice a pair of zero-splitting patterns was observed for each resonance line symmetrically with respect to the b-axis because of the monoclinic system. ⊙: efg axis.

the y-axis of the efg tensor and that of ν_2 is formed around the z-axis when η is greater than 41.2%.[11,12] Therefore, it is apparent from Fig. 1 that the z-axis of this antimony atom is almost perpendicular to the Br–Sb–Br plane and the y-axis is parallel to the bisector of the two Sb–Br bonds. Table 4 shows the angles between their efg axes determined by the Zeeman effect of NQR. Furthermore, the large values of η and e^2Qq/h of the antimony atom also support the existence of the V-shaped $SbBr_2$ unit. Figure 2 shows the orientation of the efg axes of this antimony atom as compared with that of the bridging Br atom existing in Al_2Br_6[13] or KAl_2Br_7.[9] This figure shows that the x-axis and y-axis of these two bridging atoms are reversed, although their bond angles are nearly equal to each other. The efg axes for the bridging Br atom have been explained by assuming that the Br atom forms sp^3 hybridized orbitals with two lone pair orbitals.[14,15] On the other hand, in order to explain the reversed orientation of the x- and y-axes at the Sb atom, sp^2 hybridized orbitals

Table 4. The angles between efg principal axes for the SbX_2^+ ion[a] (1) $SbBr_2^+$ (2) SbI_2^+

(1) $SbBr_2^+$	Sb z-axis	Sb y-axis	Br(5) z-axis
Sb y-axis	90.0°		
Br(5) z-axis	90.0°	48.6°	
Br(6) z-axis	90.0°	48.8°	97.3°
(2) SbI_2^+	Sb z-axis	Sb y-axis	I(5) z-axis
Sb y-axis	90.0°		
I(5) z-axis	90.1°	56.4°	
I(6) z-axis	89.9°	42.7°	99.0°

a) Experimental error was estimated to be ±0.2°.

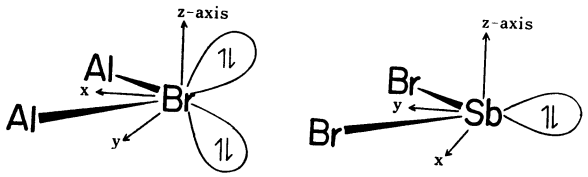

Fig. 2. efg axes with respect to the bridging plane. (a) Bridging Br atom in the Al_2Br_6 crystal and (b) antimony in the $SbBr_2^+$ ion.

with C_{2v} symmetry are adopted by assuming no hybridization of the d orbitals. The orthonormal orbitals at the Sb atom are expressed as follows:

$$\phi_1 = \psi_z,$$
$$\phi_2 = \alpha\psi_s - (1-\alpha^2)^{1/2}\psi_y,$$
$$\phi_3 = (2)^{-1/2}\{(1-\alpha^2)\psi_s + \alpha\psi_y - \psi_x\},$$
$$\phi_4 = (2)^{-1/2}\{(1-\alpha^2)\psi_s + \alpha\psi_y + \psi_x\},$$

with $$\alpha = \cot 2\gamma,$$

where ψ_s, ψ_x, ψ_y, and ψ_z are the 5s, $5p_x$, $5p_y$, and $5p_z$ orbitals of the antimony atom and 2γ is the bond angle ∠BrSbBr. The ∠BrSbBr angle was determined to be 97.3° by measuring the ^{81}Br Zeeman effect. The lone pair orbital ϕ_2 contains two electrons and has a large portion of s orbital; the electrons can be regarded as an inert pair of the Sb atom. The sigma-bonding orbitals ϕ_3 and ϕ_4 are used to form bonds with two Br atoms. The populations of these orbitals are roughly estimated to be 0.55 from the ionic character of the Sb–Br bond, which was determined by the NQR parameters of ^{81}Br by assuming 15% s-electron character for the bonding orbital of the Br atom. Then, the populations of the orbitals ϕ_1, ϕ_2, and ϕ_3 $(=\phi_4)$ are

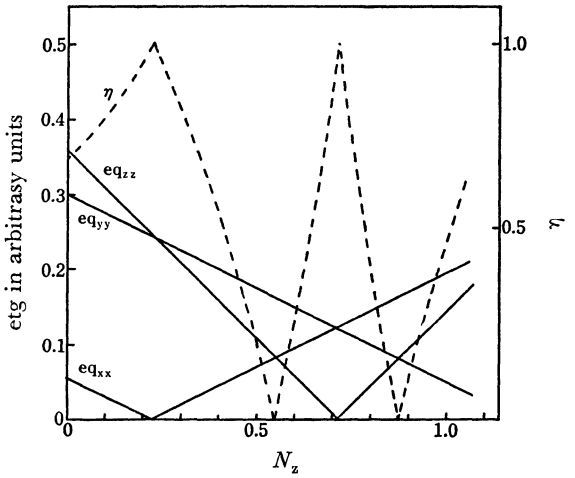

Fig. 3. Dependence of the efg at the Sb site on the population of the ϕ_1 orbital. If the population is smaller than 0.23, the observed orientation of the efg axes is consistent with this calculation.

assumed to be N_z, 2, and 0.55, respectively. Using the Townes-Dailey theory, the efg at the Sb site can be expressed as a function of N_z, where x-, y-, and z-axes are chosen as shown in Fig. 2. At N_z=0.11, the observed asymmetry parameter and the orientation of the efg tensor could be explained satisfactorily. This electronic configuration is consistent with that expected from the $SbBr_2^+$ ion, because the outer electron configuration of the Sb^+ ion is $5s^25p^2$. Further calculation is obstracted because of the lack of accurate information on the crystal structure and the quadrupole coupling constant for a 5p electron of antimony.

Figure 4 shows the zero-splitting patterns of the Br(1)—Br(4). The angles between their z-axes are distributed from 103.9 to 118.1°. This fact suggests the existence of a distorted tetrahedral $AlBr_4^-$ ion, although their efg z-axes somewhat deviate from the Br–Al bond axes because of the large η value. Figure 5

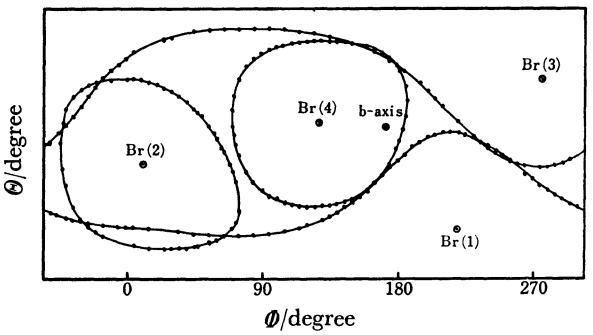

Fig. 4. Zero-splitting loci for the ^{81}Br(1)—Br(4) lines in the $AlBr_3 \cdot SbBr_3$ crystal. In practice a pair of zero-splitting patterns was observed for each resonance line symmetrically with respect to the b-axis. ⊙: efg axis.

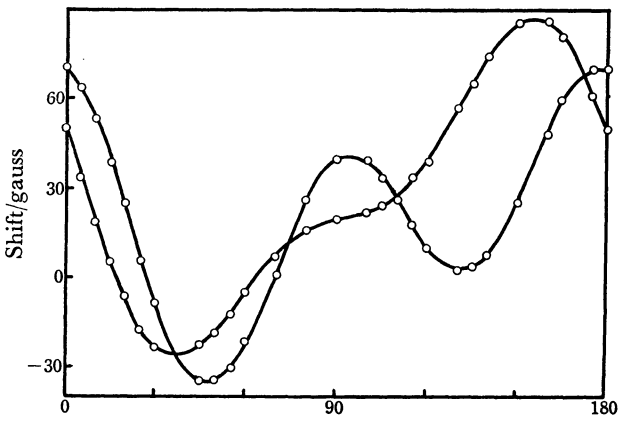

Fig. 5. The second order quadrupole effect in ^{27}Al NMR for the $AlBr_3 \cdot SbBr_3$ crystal.

shows the ^{27}Al NMR rotation pattern of the central line $(-1/2 \leftrightarrow +1/2)$, and in this case the rotation axis was arbitrarily chosen. Because of the monoclinic system, two central lines corresponding to different orientations of their efg tensors were observed. The e^2Qq/h and η thus obtained also support the distortion of the $AlBr_4^-$ ion from the regular tetrahedron, but the e^2Qq/h value is smaller than that of tetrahedrally bonded aluminum in the Al_2Br_6[14] or KAl_2Br_7[9] crystal.

From these findings it seems reasonable to propose that the $AlBr_3 \cdot SbBr_3$ crystal consists of the $SbBr_2^+$ and $AlBr_4^-$ ions and these ions are linked together by weak bonds between the Sb atom in $SbBr_2^+$ and the Br atom in $AlBr_4^-$. The lower population for the ϕ_1 orbital than ϕ_3 or ϕ_4 may suggest the existence of a weak bond between the Sb atom and the Br atom of the $AlBr_4^-$ ion. According to X-ray crystal analysis, similar structures are reported for $AlCl_3 \cdot ICl_3$,[16] $SbCl_5 \cdot ICl_3$,[16] and $AlCl_3 \cdot TeCl_4$.[17] These crystals consist of ion pairs, $AlCl_4^-ICl_2^+$, $SbCl_6^-ICl_2^+$, and $AlCl_4^-TeCl_3^+$, in which cations and anions are linked by weak bonds through the Cl atoms of the anions.

$AlI_3 \cdot SbI_3$. In the case of ^{127}I and ^{121}Sb (both I=5/2), a pair of NQR lines, $\nu_1(\pm 1/2 \leftrightarrow \pm 3/2)$ and $\nu_2(\pm 3/2 \leftrightarrow \pm 5/2)$, were observed. Zero-splitting patterns were observed for the six ν_1 transitions of the ^{127}I nuclei and for the ν_1 and ν_2 transitions of the ^{121}Sb nuclei.

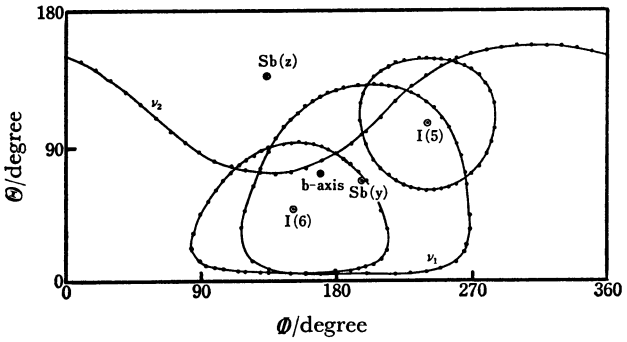

Fig. 6. Zero-splitting loci for the $^{127}I(5)$, $^{127}I(6)$, $^{121}Sb(\pm 1/2 \leftrightarrow \pm 3/2)$, and $^{121}Sb(\pm 3/2 \leftrightarrow \pm 5/2)$ lines in the $AlI_3 \cdot SbI_3$ crystal at room temperature. In practice a pair of zero-splitting patterns was observed for each resonance line symmetrically with respect to the b-axis because of the monoclinic system. ⊙: efg axis.

Therefore, the assignment of the pair ν_1 and ν_2 can be determined on the basis of the asymmetry parameter from the zero-splitting pattern. For the ^{127}I and ^{121}Sb nuclei the two values of the asymmetry parameter were independently calculated from the results of the Zeeman effect and from the frequency ratio of the pair, as shown in Table 1. The NQR parameters of this compounds are similar to that of the $AlBr_3 \cdot SbBr_3$ crystal, *i.e.*, this compound is expected to consist of the ion pair of SbI_2^+ and AlI_4^-. Figure 6 shows the zero-splitting patterns of $^{121}Sb(\pm 1/2 \leftrightarrow \pm 3/2)$, $^{121}Sb(\pm 3/2 \leftrightarrow \pm 5/2)$, $^{127}I(5)(\pm 1/2 \leftrightarrow \pm 3/2)$, and $^{127}I(6)(\pm 1/2 \leftrightarrow \pm 3/2)$, which arise from one SbI_2 unit. From the orientations of the efg tensors, the V-shaped SbI_2 unit has the geometry shown in Table 4. The z-axis of the Sb atom is almost perpendicular to the I–Sb–I plane, whereas the y-axis deviates about 7 degrees from the bisector of the two Sb–I bonds to the z-axis of the I(6) atom within the ISbI plane. This may be due to the fact that the two Sb–I bonds somewhat differ from each other, as is obvious from the e^2Qq/h of the I(5) and I(6) atoms.

$AlBr_3 \cdot BiBr_3$. The NQR spectra for this compound are different from those of the former compounds in the following points. (1) The asymmetry parameter of the ^{209}Bi atom is relatively small. (2) Only the Br(6) atom can be regarded as a terminal atom bonded to the Bi atom. (3) The Br(5) atom yields a somewhat smaller

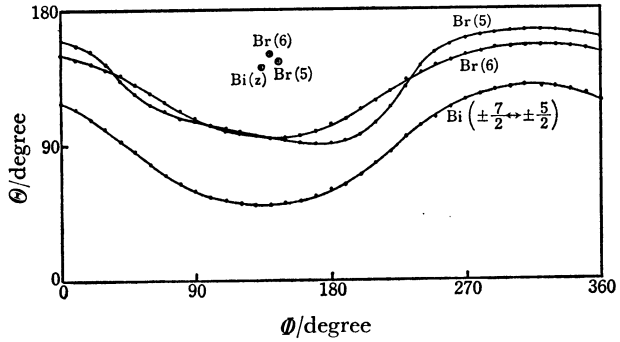

Fig. 7. Zero-splitting loci for the $^{81}Br(5)$, $^{81}Br(6)$, and ^{209}Bi $(\pm 5/2 \leftrightarrow \pm 7/2)$ lines in the $AlBr_3 \cdot BiBr_3$ crystal. ⊙: efg axis.

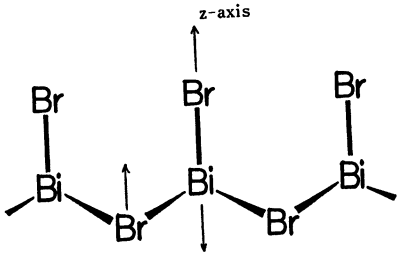

Fig. 8. Proposed structure for the $BiBr_2^+$ ion. The arrows indicate efg z-axes.

e^2Qq/h value compared with that of $BiBr_3$,[18] so that it must form a bridging bond of the type Bi–Br–Bi because of its large η.

Figure 7 shows the zero-splitting patterns of the ^{209}Bi $(\pm 7/2 \leftrightarrow \pm 9/2)$, $^{81}Br(5)$, and $^{81}Br(6)$ resonance lines. Each resonance line yields only one zero-splitting pattern. This fact suggests that the crystal belongs to a triclinic system. As is obvious from this figure, the z-axes of the three atoms are nearly parallel, within 9 degrees. On the basis of these findings, it is supposed that the $BiBr_2^+$ ions form a chain-like structure such as is shown in Fig. 8.

References

1) J. Kendall, E. D. Crittenden, and H. K. Miller, *J. Am. Chem. Soc.*, **45**, 963 (1923).
2) A. T. Nizhnik, *J. Gen. Chem.*, **7**, 1935 (1937).
3) E. Chemouni, M. H. Maglione, and A. Potier, *Bull. Soc. Chim. Fr.*, **1970**, 489.
4) V. P. Spiridonov and A. S. Malkova, *Zh. Strukt. Khim.*, **10**, 332 (1969).
5) E. Chemouni and A. Potier, *J. Inorg. Nucl. Chem.*, **33**, 2353 (1971).
6) T. Okuda, K. Yamada, H. Ishihara, and H. Negita, *Chem. Lett.*, **1975**, 785.
7) T. P. Das and E. L. Hahn, "Nuclear Quadrupole Resonance Spectroscopy," Solid State Physics, Suppl. 1, Academic Press, New York (1957).
8) G. M. Volkoff, *Can. J. Phys.*, **31**, 820 (1953).
9) K. Yamada, *J. Sci. Hiroshima Univ., Ser. A*, **41**, 77 (1977).
10) T. Okuda, H. Terao, O. Ege, and H. Negita, *Bull. Chem. Soc. Jpn.*, **43**, 2398 (1970).
11) K. Shimomura and N. Inoue, *J. Phys. Soc. Jpn.*, **14**, 86 (1959).
12) T. Okuda, K. Yamada, Y. Furukawa, and H. Negita, *Bull. Chem. Soc. Jpn.*, **48**, 3480 (1975).
13) T. Okuda, H. Terao, O. Ege, and H. Negita, *J. Chem. Phys.*, **52**, 5489 (1970).
14) P. A. Casabella, P. J. Bray, and R. G. Barnes, *J. Chem. Phys.*, **30**, 1393 (1959).
15) E. A. C. Lucken, "Nuclear Quadrupole Coupling Constants," Academic Press, New York (1969).
16) C. G. Vonk and E. H. Wiebenga, *Acta Crystallogr.*, **12**, 859 (1959).
17) B. Krebs, B. Buss, and D. Altena, *Z. Anorg. Allg. Chem.*, **386**, 257 (1971).
18) Y. Furukawa, *J. Sci. Hiroshima Univ., Ser. A*, **37**, 357 (1973).
19) N. Weiden and A. Weiss, *J. Magn. Reson.*, **20**, 334 (1975).
20) S. Ogawa, *J. Phys. Soc. Jpn.*, **13**, 618 (1958).